Earth and Planetary Science Letters 432 (2015) 1–12

Contents lists available at ScienceDirect

Earth and Planetary Science Letters

www.elsevier.com/locate/epsl

Effects of the post-perovskite phase transition properties on the stability and structure of primordial reservoirs in the lower mantle of the Earth

Yang Li [a,b,*], Frédéric Deschamps [b], Paul J. Tackley [a]

[a] Institute of Geophysics, Department of Earth Sciences, ETH Zurich, Sonnegstrasse 5, 8092 Zurich, Switzerland
[b] Institute of Earth Sciences, Academia Sinica, 128 Academia Road Sec. 2, Nangang, Taipei 11529, Taiwan

ARTICLE INFO

Article history:
Received 31 March 2015
Received in revised form 28 August 2015
Accepted 25 September 2015
Available online xxxx
Editor: B. Buffett

Keywords:
thermo-chemical mantle convection
post-perovskite
primordial reservoir

ABSTRACT

Two key features of the lowermost Earth's mantle are the presence of Large Low Shear Velocity Provinces (LLSVPs), which may be reservoirs of primordial, chemically distinct material, and the phase change from perovskite (pv) to post-perovskite (pPv), which may occur at lowermost mantle conditions. However, the influence of this phase change on the shape, dynamics, and stability of chemically distinct reservoirs is not well constrained. Here, we performed numerical experiments of thermo-chemical convection in 2-D spherical annulus geometry to investigate the effects on thermo-chemical structure in the lower mantle of three parameters affecting the pPv phase change: the core–mantle boundary (CMB) temperature (T_{CMB}), the viscosity ratio between pv and pPv ($\Delta\eta_{pPv}$), and the Clapeyron slope of the pPv phase transition (Γ_{pPv}). Our results indicate that increasing CMB temperature increases the wavelength of the primordial reservoirs. Furthermore, a high CMB temperature promotes the development of plumes outside the reservoir of primordial material. High CMB temperature and large Clapeyron slope both favour the formation of pPv patches and of a double-crossing of the phase boundary, thus preventing the formation of continuous layer of pPv above the CMB. Combined with a low CMB temperature and/or a low Clapeyron slope of the pPv phase transition, a full layer of weak pPv above the CMB strongly enhances the mixing efficiency of primordial material with ambient regular mantle material, which may not allow the generation of large reservoirs. Based on our experiments, we conclude that the models of convection best describing the Earth's mantle dynamics include a large pPv Clapeyron slope (typically in the range of 13–16 MPa/K), and a moderate CMB temperature (around 3750 K). Our models do not provide further constraints on the value of the pPv viscosity, both regular and low values giving similar results on stability and structure of large primordial reservoirs for models with a moderate CMB temperature and large Clapeyron slope, but more plumes can be observed outside these large reservoirs in the cases with regular pPv than those in the cases with weak pPv.

1. Introduction

One of the most important discoveries of the past decade in mineral physics is the phase change from perovskite (pv) to post-perovskite (pPv), which may occur under the conditions of the lowermost mantle of the Earth (Murakami et al., 2004; Oganov and Ono, 2004; Tsuchiya et al., 2004). This phase transition was predicted by Sidorin et al. (1999), who noted that an exothermic phase change above the core–mantle boundary (CMB) would explain the D'' discontinuity observed by seismologists better than a chemically distinct layer. Since its discovery, post-perovskite was found to bear properties compatible with the properties of the D'' region. In particular, the shear modulus of pPv is larger than that of pv, implying that shear-waves travel faster in pPv regions (e.g., Caracas and Cohen, 2005; Mao et al., 2007; Stackhouse and Brodholt, 2007). Recent seismic observations (Cobden and Thomas, 2013) suggest that the D'' discontinuity may however have different origins depending on the polarities of P- and S-waves, and that the pPv phase transition may be a good candidate for regions where these polarities are opposite. A key property of the pPv phase transition is its large Clapeyron slope, around 8–10 MPa/K (Oganov and Ono, 2004), or even more according to recent estimates (Tateno et al., 2009; Hernlund, 2010), implying that pPv should not be stable in hot regions, which would explain why the

* Corresponding author at: Institute of Earth Sciences, Academia Sinica, 128 Academia Road Sec. 2, Nangang, Taipei 11529, Taiwan.
E-mail address: yli@earth.sinica.edu.tw (Y. Li).

http://dx.doi.org/10.1016/j.epsl.2015.09.040
0012-821X/

seismic discontinuity atop D'' is not ubiquitous. Interestingly, pPv is a strongly anisotropic mineral, and its presence may thus explain the anisotropy observed in the D'' region (Wookey et al., 2005).

Seismic tomography models further reveal two Large Low Shear Velocity Provinces (LLSVPs) in the lowermost mantle beneath Africa and the Pacific (e.g., Masters et al., 2000; Trampert et al., 2004; Ni et al., 2002; He and Wen, 2012). Cluster analysis (Lekic et al., 2012) and the fact that they are also observed by normal mode tomography (Ishii and Tromp, 1999; Trampert et al., 2004; Mosca et al., 2012) indicate that LLSVPs are robust features, not artifacts. Furthermore, probabilistic tomography (Trampert et al., 2004; Mosca et al., 2012) suggest that they are hotter and chemically distinct compared to the ambient mantle. Since the phase change from perovskite (pv) to post-perovskite (pPv) is mainly expected to occur in cold regions of the lowermost mantle, pPv may not be found within LLSVPs. This is in agreement with the most recent thermo-chemical distributions deduced from probabilistic tomography (Mosca et al., 2012). If it is present outside LLSVPs, pPv may explain the anti-correlation between shear-wave and bulk sound velocity anomalies (Hutko et al., 2008; Davies et al., 2012).

The presence of post-perovskite may have some substantial influences on mantle dynamics. It has been pointed out, for instance, that the distributions of dense material and post-perovskite are anti-correlated (Nakagawa and Tackley, 2005, 2006), and the spectra of chemical anomalies are strongly influenced by the topography of the post-perovskite phase transition (Nakagawa and Tackley, 2006). Furthermore, due to its large Clapeyron slope, the post-perovskite phase transition may be responsible for specific structures such as double-crossings in warm regions (Hernlund et al., 2005). It is therefore important to properly describe the interactions between the pPv phase transition and the LLSVPs. This, in turn, requires a good knowledge of the properties of pPv and of the conditions under which it appears, including the temperature at the CMB, the Clapeyron slope of the pPv phase transition, and the viscosity of the pPv relative to that of pv. These parameters, however, remain poorly constrained.

The CMB temperature provides important constrains on the thermal structure of Earth's mantle. Previous laser-heated diamond-anvil cell (DAC) experiments indicated that the solidus temperature of primitive mantle is about 4200 K at the CMB (e.g., Zerr et al., 1998; Fiquet et al., 2010; Andrault et al., 2011). This high CMB temperature indicates that part of the CMB region is in the perovskite stability field, thus preventing a global layer of pPv covering the CMB. However, a recent study by Nomura et al. (2014) suggests that a natural primitive mantle (pyrolite) with 400 ppm H_2O could result in a much lower CMB temperature (3570 ± 200 K) compared to the previously assumed range of values.

The viscosity contrast between pv and pPv remains a matter of debate. Some experimental studies (e.g., Yoshino and Yamazaki, 2007; Hunt et al., 2009), as well as theoretical calculations by Ammann et al. (2010) based on the first-principle methods, reported a weak pPv viscosity, by a factor of $O(10^3)$ to $O(10^4)$ lower than that of pv. A low viscosity of pPv is consistent with recent geoid modelling, which requires colder regions of the deepest lower mantle to be weaker than hotter regions (Cadek and Fleitout, 2006). Meanwhile, some other studies give opposite results favouring more viscous pPv (Karato, 2011).

The Clapeyron slope of the phase transition from pv to pPv also varies in different experimental studies from early measured values of 8–10 MPa/K (e.g., Oganov and Ono, 2004) to the current preferred value of 13 MPa/K or higher (e.g., Tateno et al., 2009; Hernlund, 2010).

In this study, we perform a series of numerical experiments of thermo-chemical convection to investigate the influence of each of the three parameters discussed above on mantle convection. We focus in particular on their effects on the stability and structure of the primordial reservoirs in the lower mantle.

2. Numerical experiments set up

The numerical experiments are performed with StagYY (Tackley, 2008), which solves the conservation equations of mass, momentum, energy, and composition for an anelastic compressible fluid with infinite Prandtl number. Calculations are performed in 2-D spherical annulus geometry (Hernlund and Tackley, 2008) with a ratio between inner and outer radii of $f = 0.55$, matching the Earth's mantle.

The viscosity is assumed to depend on temperature, depth, phase, and yield stress. A viscosity jump of 30 is imposed at the boundary between upper and lower mantles. Viscosity is thus given by

$$\begin{aligned}
&\eta_b(z, T, \Gamma_{pPv}) \\
&\quad = \eta_0\big[1 + 29H(z - 660)\big] \\
&\qquad \times \exp\left[\Gamma_{pPv}\ln(\Delta\eta_{pPv}) + V_a\frac{z}{D} + E_a\frac{\Delta T_S}{(T + T_{off})}\right] \\
&\eta_Y = \frac{\sigma_0 + \sigma_i P}{2\dot{e}} \\
&\eta = \frac{1}{\left(\frac{1}{\eta_b(z,T,\Gamma_{pPv})} + \frac{1}{\eta_Y}\right)}
\end{aligned} \tag{1}$$

where η_0 is the reference viscosity (taken at temperature $T = 1600$ K and depth $z = 0$ km), H is the Heaviside step function, and $\Delta\eta_{pPv}$ is the viscosity jump between perovskite and post-perovskite, which is equal to 1 for regular pPv, and 1/1000 in the case of weak pPv. V_a and E_a are the non-dimensional activation volume and energy, controlling viscosity variations with depth and temperature, respectively. T_{off} is the offset temperature, which reduces the viscosity jump through the top thermal boundary layer. Here, we set the value of this parameter to $0.88\Delta T_S$. The yield stress helps to build plate-like behaviour at the top of the domain. Here, we define the yield stress by imposing its surface value σ_0, and its pressure gradient σ_i. The yield viscosity η_Y, is defined as the ratio between the yield stress and the second invariant of the strain rate tensor $\dot{e}$. To avoid numerical difficulties, the viscosity is truncated between 10^{-3} and 10^5 of the reference viscosity.

The reference Rayleigh number is defined as:

$$Ra_{ref} = \frac{\alpha_s g \rho_s \Delta T_s D^3}{\eta_0 \kappa_s} \tag{2}$$

where α_s is the surface thermal expansivity, g the acceleration of gravity, ΔT_s the super-adiabatic temperature difference, D the mantle thickness, η_0 the reference viscosity obtained using the potential temperature of 1600 K at the surface, and κ_s the surface thermal diffusivity. This reference Rayleigh number remains constant during the entire experiment, and in this study we prescribed $Ra_{ref} = 10^8$ for all experiments. The effective Rayleigh number Ra_{eff}, calculated with volume-averaged properties, varies with time but remains around 3×10^6 in all our calculations.

We use a phase function approach to model the perovskite to post-perovskite phase transition. This phase function is based on that in Christensen and Yuen (1985), and is defined by

$$\Gamma_{pPv}(T, z) = 0.5 + 0.5\tanh\frac{z - z_{pPv} - \gamma_{pPv}(T - T_{pPv})}{w} \tag{3}$$

where Γ_{pPv} is the phase function for post-perovskite, varying from 0 for perovskite to 1 for post-perovskite, T and z are temperature and depth, respectively, (T_{pPv}, z_{pPv}) is a point on the phase boundary, γ_{pPv} is the Clapeyron slope and w is the width of the phase

Table 1
Mantle model physical parameters.

Parameter	Symbol	Value	Units	Non-dimensional
Non-dimensional parameters				
Reference Rayleigh number	Ra_s			10^8
Buoyancy ratio	B			0.28
Volume fraction of dense material	X			0.04
Initial thickness of the dense layer	h_{DL}			0.07
Surface dissipation number	Di_S			1.2
Compositional heating ratio	RH_C	10		
Physical and thermo-dynamical parameters				
Acceleration of gravity	g	9.81	$m\,s^{-2}$	1.0
Mantle thickness	D	2891	km	1.0
Super-adiabatic temperature difference	ΔT_S	2500	K	1.0
Reference adiabat	T_{as}	1600	K	0.64
Surface density	ρ_S	3300	kg/m^3	1
CMB density	ρ_b	5610	kg/m^3	1.7
Density jump at $z = 660$ km	$\Delta\rho_{660}$	400	kg/m^3	0.1212
Surface thermal expansion	α_S	5.0×10^{-5}	K^{-1}	1.0
CMB thermal expansion	α_b	1.0×10^{-5}	K^{-1}	0.2
Surface thermal diffusivity	κ_S	6.24×10^{-7}	$m^2\,s^{-1}$	1.0
CMB thermal diffusivity	κ_b	8.74×10^{-7}	$m^2\,s^{-1}$	1.4
Clapeyron slope at $z = 660$ km	Γ_{660}	−2.5	MPa/K	-6.68×10^{-2}
Viscosity law				
Reference thermal viscosity	η_0	1.6×10^{21}	Pa s	1.0
Viscosity ratio at $z = 660$ km	$\Delta\eta_{660}$	30		
Thermal viscosity ratio	$\Delta\eta_T$	10^{10}		
Vertical viscosity ratio	$\Delta\eta_Z$	10^2		
Dimensional scalings				
Velocity	v	1.0	$cm\,yr^{-1}$	1468
Time	t	424	Gyr	1.0
Heat flux	Φ	2.6	$mW\,m^{-2}$	1.0
Internal heating rate	H	2.72×10^{-13}	$W\,kg^{-1}$	1.0

transition. In this study, the phase boundary from perovskite to post-perovskite occurs at 2650 K and 2700 km depth, which allows a double crossing in the lowermost mantle (e.g., Hernlund et al., 2005) in some cases.

A layer of dense material, modelling primitive material, of thickness $h_{DL} = 0.07$ (corresponding to 5% in volume), is initially imposed at the bottom of the mantle. The density contrast between primordial and regular material is controlled by the buoyancy ratio (B):

$$B = \frac{\Delta\rho_C}{\alpha_s \rho_s \Delta T_s} \tag{4}$$

where $\Delta\rho_C$ is the density difference between the dense and regular material. In this study, we fix B to 0.28. For a superadiabatic temperature difference $\Delta T_S = 2500$ K and thermal expansion $\alpha_s = 5.0 \times 10^{-5}$ (i.e., taken at $z = 0$ and $T = 1600$ K), this corresponds to a density contrast of 115 kg/m^3. Taking PREM as a reference, this leads to a relative density anomaly of about 2.3% at the bottom of the mantle, a value that is consistent with current estimates of density anomalies in the lower mantle (e.g., Trampert et al., 2004; Mosca et al., 2012). The values of other physical parameters are listed in Table 1.

The initial radial temperature profile is adiabatic with a potential temperature of 2000 K, and the shell is heated both from the bottom and from within. The numerical resolution is 96×768, and is radially refined in the top and bottom 150 km. At best, the grid refinement at top and bottom leads to 6 km thick cells. A collection of 2.2 million tracers is used to track composition. The compositional field is calculated from the fraction of dense tracers at each location, and varies between 0 for regular material and 1 for primordial material.

To estimate the degree of mixing between dense and regular materials, we use the average depth of dense material, as defined by Deschamps and Tackley (2008):

$$< h_c > = \frac{1}{V} \int_V C(r, \theta, \phi) r dV . \tag{5}$$

Values of $< h_c >$ around 0.57 or more indicate efficient mixing, whereas for stable layering $< h_c >$ is equal to 0.045. For stable reservoirs of dense material, $< h_c >$ is in between the values for efficient mixing and stable layering.

3. Results

Using the setup outlined in Section 2, we performed a series of numerical experiments in which we varied the temperature at the CMB (T_{CMB}), the viscosity contrast between pv and pPv ($\Delta\eta_{pPv}$), and the Clapeyron slope of the pPv phase transition (Γ_{pPv}). Model parameters are listed in Table 1, and properties of the runs discussed in this section are detailed in Table 2.

3.1. Reference case

We first define a reference case (case M1 in Table 2), for $T_{CMB} = 3750$ K, $\Delta\eta_{pPv} = 1$, and $\Gamma_{pPv} = 13$ MPa/K. Fig. 1d–f show snapshots of the temperature, composition and phase field of the reference case at $t = 4.5$ Gyr. Two large reservoirs of dense primordial material are generated above the CMB about 2 Gyr from the beginning of the run, and remain stable with a degree-two structure for the rest of the experiment. Fig. 2c shows the average area covered by primordial material at the CMB (solid lines) and 300 km above it (dashed lines). For the reference case (black lines) at $t = 4.5$ Gyr, primordial material covers about 1/3 of the total

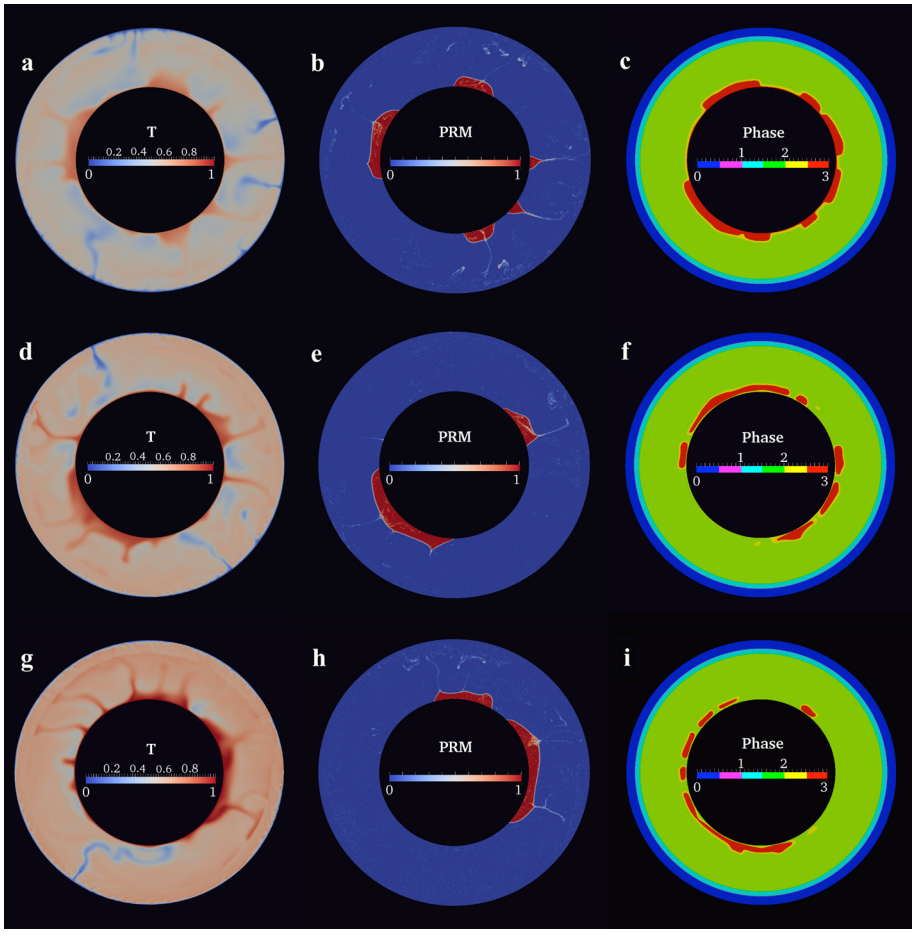

Fig. 1. Snapshots taken at $t = 4.5$ Gyr from cases with regular post-perovskite, $\Gamma_{pPv} = 13$ MPa/K, and different CMB temperatures. From top to bottom: $T_{CMB} = 3350$, 3750, 4200 K; from left to right: superadiabatic temperature, composition, phase fields. For the phase field, the colour code ranges from 0 to 3 for olivine, spinel, perovskite, and post-perovskite, respectively. (For interpretation of the references to colour in this figure legend, the reader is referred to the web version of this article.)

Table 2
Cases used in this study.

Name	botT	$\Delta\eta_{ppv}$	Γ_{ppv}
L1	3350 K	1	13 MPa/K
L2	3350 K	1	8 MPa/K
L3	3350 K	1	16 MPa/K
L4	3350 K	10^{-3}	13 MPa/K
L5	3350 K	10^{-3}	8 MPa/K
L6	3350 K	10^{-3}	16 MPa/K
M1	3750 K	1	13 MPa/K
M2	3750 K	1	8 MPa/K
M3	3750 K	1	16 MPa/K
M4	3750 K	10^{-3}	13 MPa/K
M5	3750 K	10^{-3}	8 MPa/K
M6	3750 K	10^{-3}	16 MPa/K
H1	4200 K	1	13 MPa/K
H2	4200 K	1	8 MPa/K
H3	4200 K	1	16 MPa/K
H4	4200 K	10^{-3}	13 MPa/K
H5	4200 K	10^{-3}	8 MPa/K
H6	4200 K	10^{-3}	16 MPa/K

area at the CMB, and 1/4 300 km above it, leading to reservoirs with relatively sharp edges. Plumes are generated at the top of the reservoirs and at their margins, entraining upwards small fractions of dense material. Furthermore, a few plumes are also generated outside the reservoirs of primordial material. Post-perovskite is stable only outside the reservoirs of primordial material, which are hotter than average, and away from the additional plumes generated outside these reservoirs. As a result pPv is distributed in discontinuous patches above the CMB. We also observe a 'double-crossing' of the pPv phase change at the edges of these patches.

3.2. Effects of the core–mantle boundary temperature

We then performed experiments in which we varied the CMB temperature to explore its dynamical influence on the stability and structure of the reservoirs of primordial material. We considered three values of T_{CMB}: 3350 K, 3750 K (corresponding to the reference case), and 4200 K, sampling the range of values estimated from mineral physics experiments. In all three experiments, the viscosity of pPv is equal to that of pv ($\Delta\eta_{pPv} = 1$), and the Clapeyron slope is $\Gamma_{pPv} = 13$ MPa/K, as in the reference case.

Fig. 1 shows the temperature, composition and phase fields for three cases with different CMB temperatures. We observe strong differences in the pPv stability field, in the size and distribution of reservoirs of primitive material, and in the appearance of plumes, depending on the CMB temperature. For the lowest CMB temperature we considered ($T_{CMB} = 3350$ K), the CMB is fully covered by post-perovskite (Fig. 1c), including at the bottom of the reservoirs of primordial material, and the thickness of the pPv layer laterally varies with local temperature. Thicker layers are found in the colder-than-average regions, where cold downwellings (modelling subducted slabs) reach the lower mantle and spread along the CMB. As one would expect, the area covered by pPv decreases with increasing CMB temperature, while the phase change occurs deeper and the pPv piles become thinner. For instance, in reservoirs of dense material, which are hotter than their surroundings,

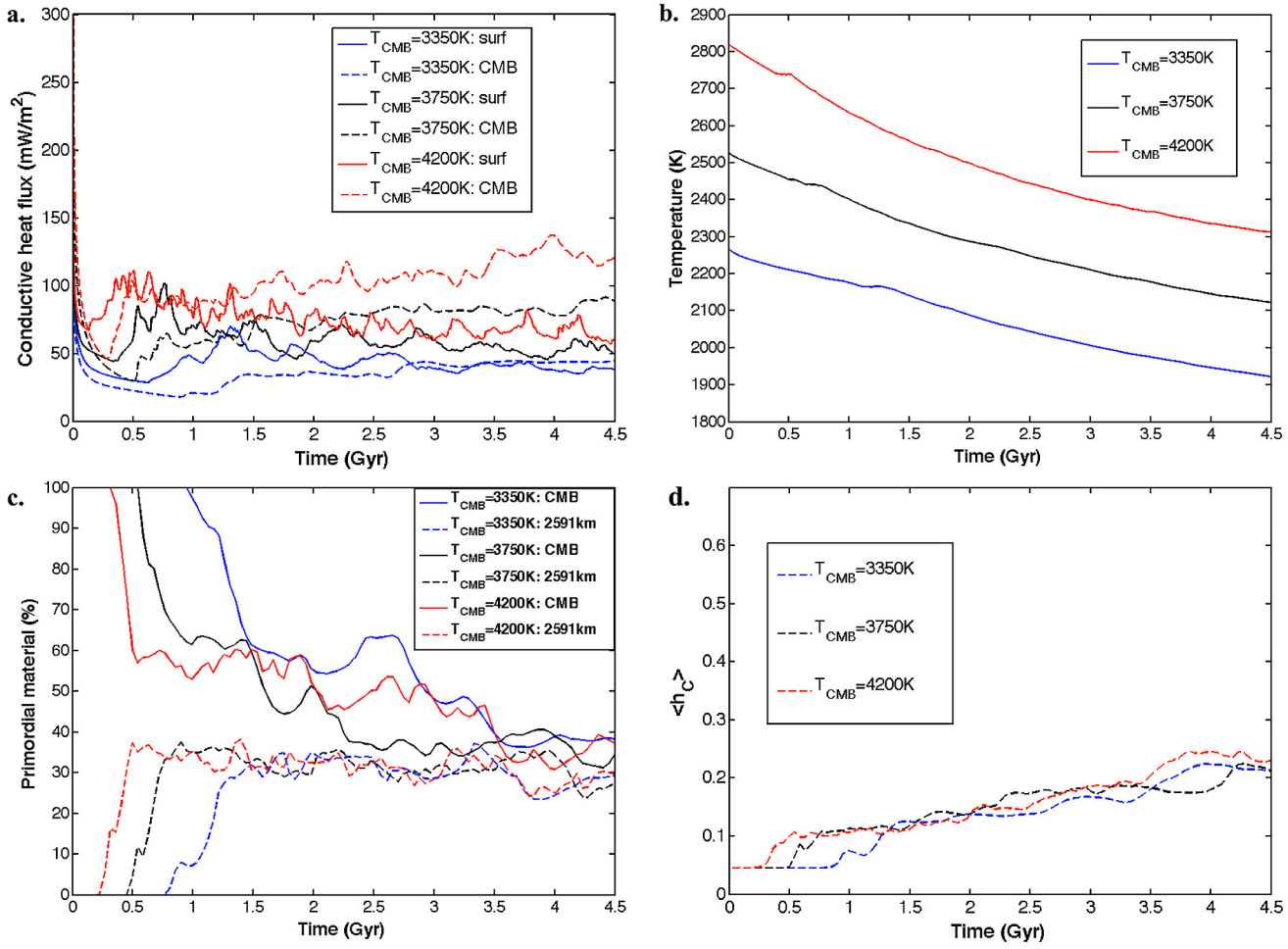

Fig. 2. (a) Surface and CMB heat flux as a function of time. (b) Volume-averaged mantle temperature as a function of time. (c) Percentage of area at the CMB and 300 km above the CMB covered by primordial material as a function of time. (d) The average altitude of primordial material as a function of time for experiments shown in Fig. 1. (For interpretation of the colours in this figure, the reader is referred to the web version of this article.)

pPv is stable only in a thin layer above the CMB. In contrast, as the CMB temperature increases, pPv is only stable outside the reservoirs of dense material, forming discontinuous patches (Figs. 1f and 1i). Double-crossing may also appear, either at the edge of the patches for an intermediate CMB temperature (Fig. 1f), or within them (Fig. 1i), for a high CMB temperature.

Increasing the CMB temperature further affects the size, structure, and distribution of the primordial reservoirs, in that the wavelength of these reservoirs increases with increasing CMB temperature (Fig. 1). For a high CMB temperature, the mantle temperature is also higher (i.e., Fig. 2b), which reduce the stress close to the surface, and oppose the formation of downwellings. A low CMB temperature ($T_{CMB} = 3350$ K), on the contrary, favours the development of cold downwellings (modelling subducted slabs) at the top of the 2D-annulus shell (Fig. 1a). Because the geometry and distribution of reservoirs of primordial material are controlled by the location of downwellings, which are pushing primordial material aside as they arrive at the bottom of the shell (e.g., Y. Li et al., 2014b), a larger number of downwellings favours in turn the formation of several small scale reservoirs (Fig. 1b). In contrast, for an intermediate CMB temperature ($T_{CMB} = 3750$ K), as in our reference case, two antipodal large primordial reservoirs are generated (Fig. 1e), while for a high CMB temperature ($T_{CMB} = 4200$ K), we observe even larger primordial reservoirs with a roughly degree-1 distribution. Figs. S1–S3 show the time evolution of thermal, chemical, and phase structures during the last 1 Gyr in the calculations. Similar to our previous studies (Y. Li et al., 2014a, 2014b), we observe that the reservoirs of dense material can be maintained in the lower mantle for a long period of time, while their locations migrate laterally and their shapes slightly change with time.

The CMB temperature finally has some important consequences for instabilities from the bottom thermal boundary layer (TBL). For $T_{CMB} = 3350$ K, plumes are rising mainly from the top of the primordial reservoirs (Fig. 1a). In contrast, for CMB temperatures of 3750 K (Fig. 1d) and 4200 K (Fig. 1g), plumes are also generated from outside these reservoirs, the number of such plumes increasing with T_{CMB}. The temperature at the feet of these plumes is higher than the surroundings, inducing gaps in the pPv layer. The CMB heat flux (Fig. 2a, dashed lines) further indicates that increasing T_{CMB} promotes the development of instabilities in the bottom TBL. For $T_{CMB} = 3350$ K, the bottom heat flux is nearly constant in the time interval 1.5–4.5 Gyr, at around 40 mW/m^2. With increasing T_{CMB}, the time-averaged heat flux strongly increases (up to 140 mW/m^2 for $T_{CMB} = 4200$ K), and its time variations have larger amplitudes. Fig. 2b, which plots the volume-averaged mantle temperature as a function of time, indicates that the cooling rate is not very sensitive to the CMB temperature. Higher values of T_{CMB} lead to slightly faster cooling, but the temperature drop over the entire experiments remains around 450 K for all cases.

Fig. 2c shows the percentage of the area covered by primordial reservoirs at the CMB and 300 km above the CMB, and Fig. 2d shows the average altitude of primordial material for the three cases shown in Fig. 1. Although the CMB temperature and the wavelength of primordial reservoirs are different in these cases,

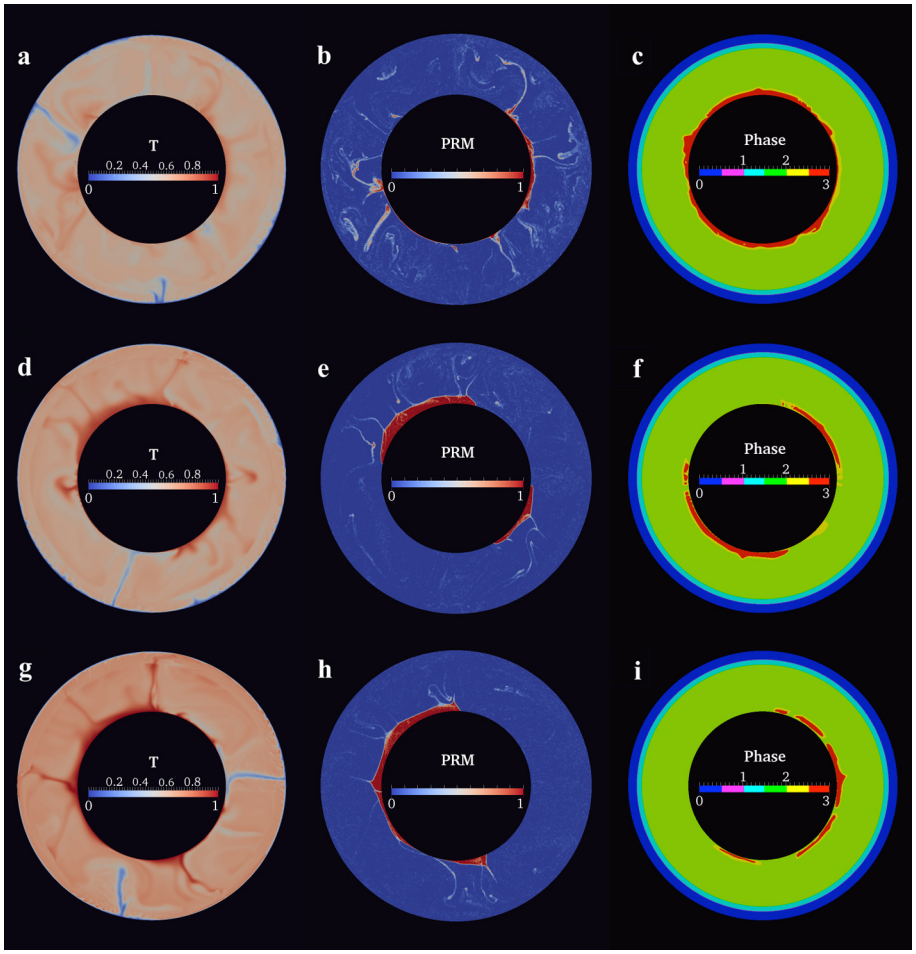

Fig. 3. Snapshots taken at $t = 4.5$ Gyr from cases with weak post-perovskite, $\Gamma_{pPv} = 13$ MPa/K, and different CMB temperatures. From top to bottom: $T_{CMB} = 3350$, 3750 and 4200 K; from left to right: superadiabatic temperature, composition, phase fields. Colour scales are similar to those in Fig. 1. (For interpretation of the references to colour in this figure legend, the reader is referred to the web version of this article.)

the total areas covered by primordial material are very similar to each other. The average altitude of dense material is also unaffected by the value of T_{CMB}, indicating that the entrainment of dense material is similar in the three cases considered here. This is due to the fact that the buoyancy ratio, which is the most important parameter controlling the stability of the primordial reservoirs (e.g., McNamara and Zhong, 2005; Deschamps and Tackley, 2009; Y. Li et al., 2014b), is the same for the three cases shown here. Its value ($B = 0.28$) allows primordial reservoirs in the lower mantle to be maintained.

3.3. *Effects of viscosity contrast between pv and pPv*

The influence of the viscosity contrast between pv and pPv is illustrated in Figs. 3 and 4 for the three values of the CMB temperature considered in Section 3.2.

Fig. 1d–f and Fig. 3d–f compare thermo-chemical structures obtained from regular and weak pPv cases with a CMB temperature equal to 3750 K. The pPv piles in the case with weak pPv are generally thinner and more continuous than those in the case with regular pPv, indicating that the mantle temperature is higher in the weak pPv case, which is also shown by the time evolution of the average mantle temperature (Figs. 2b and 4b, black lines). Comparison between Figs. 2b and 4b further indicates that the mantle cooling is slightly slower in the weak pPv case.

In both cases, we observe two large reservoirs of primordial dense material, with plumes rising from the margins and the top of these reservoirs. However, notable differences clearly appear, both in the shape of reservoirs and in the distribution of plumes and pPv. In the case with weak pPv, the primordial reservoirs are flatter. Fig. 2d and Fig. 4d, plotting the average altitude of dense material, further show that the entrainment of dense material by plumes to the upper mantle is slightly stronger in the case with weak pPv than in the case with regular pPv. In addition, the CMB heat flux in the case with weak pPv is more time-dependent and is much larger (Figs. 2a and 4a, black dashed lines). This indicates that instabilities in the bottom TBL are more easily generated if pPv is much less viscous than pv, in agreement with calculations in 3-D spherical geometry (Y. Li et al., 2014a). To check whether these results are still valid for other values of the CMB temperature, we performed experiments with low (3350 K) and high (4200 K) CMB temperatures.

Fig. 1g–i and Fig. 3g–i compare thermo-chemical structures obtained from cases with a high CMB temperature (4200 K). Most of the findings from these two experiments are consistent with those from the experiments with intermediate CMB temperature, i.e., primordial reservoirs are less stable in the case with weak pPv than in the case with regular pPv, and fewer but stronger plumes compared to the plumes are generated in the case with weak pPv. Fig. 1a–c and Fig. 3a–c compare thermo-chemical structures obtained in cases with a low CMB temperature (3350 K). In both cases, pPv fully covers the CMB region. The effects of weak pPv are more pronounced compared to the cases with $T_{CMB} = 3750$ K. With weak pPv, the reservoirs of primordial dense material nearly disappear, indicating more efficient mixing between primordial and regular materials (blue lines in Fig. 4d). Furthermore, the weak

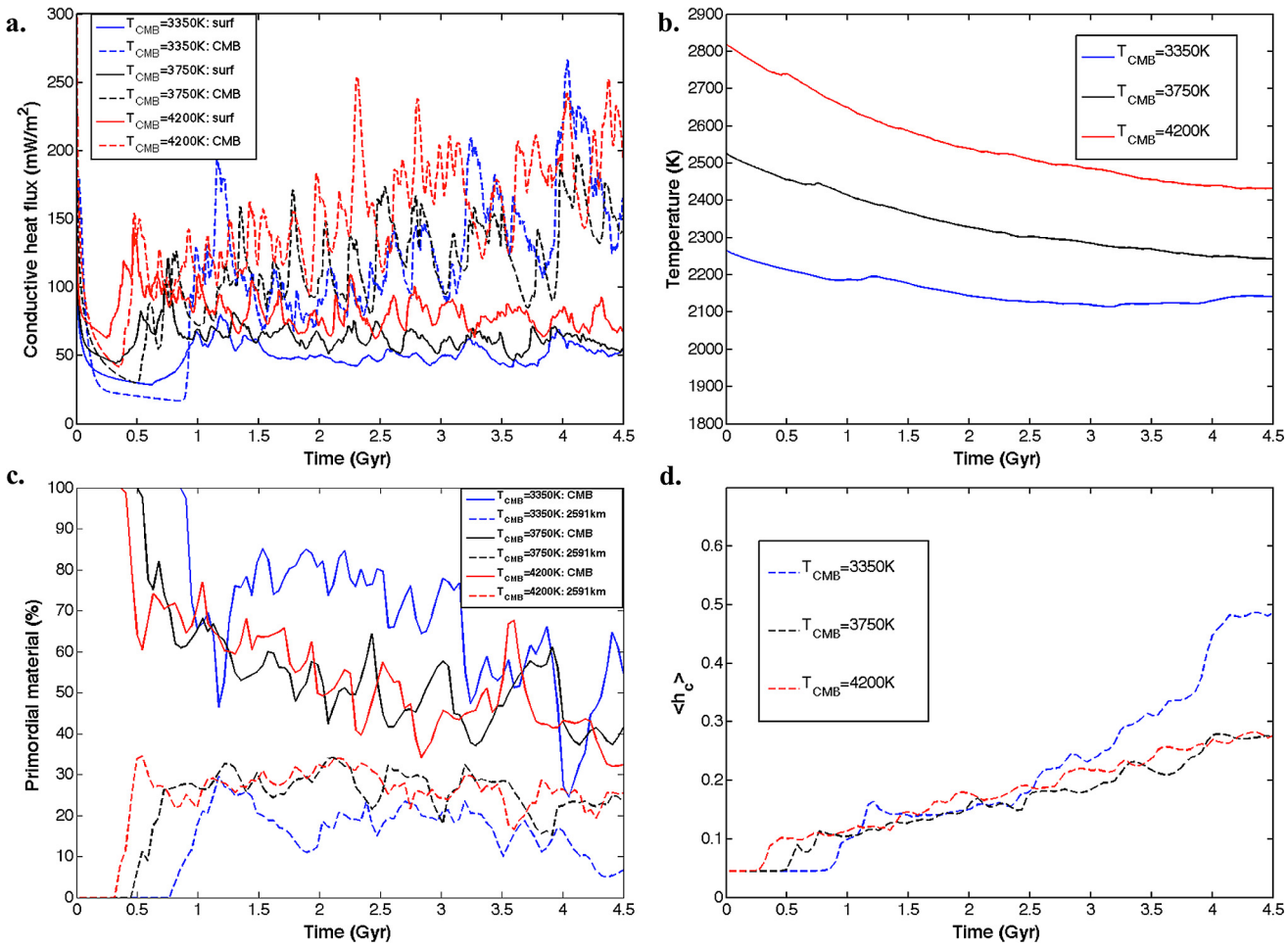

Fig. 4. (a) Surface and CMB heat flux as a function of time. (b) Volume-averaged mantle temperature as a function of time. (c) Percentage of area at the CMB and 300 km above the CMB covered by primordial material as a function of time. (d) The average altitude of primordial material as a function of time for experiments shown in Fig. 3. (For interpretation of the references to colour in this figure, the reader is referred to the web version of this article.)

pPv layer is thinner but less variable. It should be pointed out that such an ubiquitous pPv layer is unlikely in the case of the Earth's mantle, since the D'' seismic discontinuity, which is thought to be the signature of the pPv phase transition to pPv, is not observed everywhere.

Our experiments further indicate that the viscosity of pPv has an influence on the development of plumes outside the dense reservoirs. Such plumes are generated in hotter than average regions, which also cause gaps in pPv layer. With regular pPv, we observe that plumes are being generated outside dense reservoirs for all the CMB temperature we tested (Fig. 1), whereas with weak pPv they only appear for large CMB temperature (4200 K; Fig. 3). This may be related to the fact that weak pPv favours the spreading of cold downwelling around the CMB, thus preventing the development of hot instabilities in these regions, unless the CMB temperature is large enough.

3.4. Effects of Clapeyron slope of the pPv phase change

In the last series of experiments, we explore the effects of Clapeyron slope of the pPv phase change on the stability and structure of the primordial reservoirs, as well as on the pPv piles.

Fig. 5 shows that the Clapeyron slope of the pPv phase change significantly affects the shape and distributions of the pPv piles and of the primordial reservoirs in the lower mantle. In the case with $T_{CMB} = 3750$ K and a small Clapeyron slope (8 MPa/K), the pPv piles are flatter and more continuous compared to the cases with a larger Clapeyron slope (13 and 16 MPa/K), all other parameters being the same. In addition, a thin layer of pPv is present beneath the reservoirs of dense material for $\Gamma_{pPv} = 8$ MPa/K (Fig. 5c), whereas for $\Gamma_{pPv} = 13$ MPa/K (Fig. 5f) and $\Gamma_{pPv} = 16$ MPa/K (Fig. 5i), we observe a double crossing of pPv phase change. These results indicate, as one would expect, that in lowermost mantle conditions, small Clapeyron slopes favours the phase change to pPv, while large Clapeyron slopes prevent the phase change from occurring. Still in the case with $T_{CMB} = 3750$ K, plumes are generated from both within and outside the reservoirs of dense material. As noted in the previous sections, the locations where plumes are generated outside the primordial reservoirs are associated with gaps between pPv piles. Fig. 6 further indicates that the growth of instabilities in the bottom TBL is not substantially affected by the pPv Clapeyron slope. The primordial reservoirs are strongly anti-correlated with pPv piles.

Fig. 6 shows the effects of Clapeyron slope of the pPv phase transition on the weak pPv cases. In the case with $T_{CMB} = 3750$ K, pPv fully covers the CMB if the Clapeyron slope is small, and as discussed in Section 3.3, this weak pPv shell destabilises the primordial materials. The combination of a small Clapeyron slope (8 MPa/K) and weak pPv (Fig. 6a) allows primordial material to mix efficiently with the surrounding regular mantle material, leaving only very small reservoirs at the end of the run. As the Clapeyron slope increases, the CMB area covered by weak pPv decreases, and the primordial reservoirs become stable, as observed from the regular pPv cases.

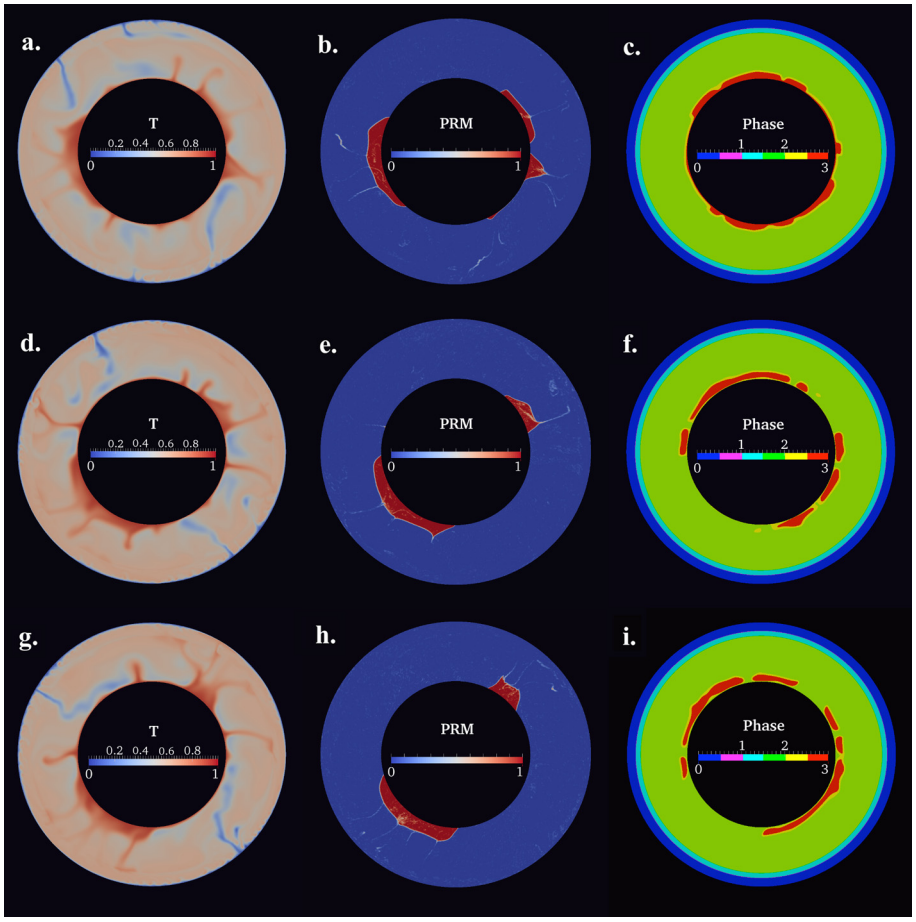

Fig. 5. Snapshots taken at $t = 4.5$ Gyr from cases with regular post-perovskite and $T_{CMB} = 3750$ K. From top to bottom: $\Gamma_{pPv} = 8, 13, 16$ MPa/K; from left to right: superadiabatic temperature, composition, and phase fields. Colour scales are similar to those in Fig. 1. (For interpretation of the references to colour in this figure legend, the reader is referred to the web version of this article.)

Finally, Fig. 7 plots cases combining a low CMB temperature (3350 K) with regular pPv. This series of experiments confirms the trend observed with an intermediate CMB temperature (Fig. 5), i.e., that increasing values of Γ_{pPv} reduces the stability field of pPv. For $\Gamma_{pPv} = 16$ MPa/K, pPv is stable only outside the reservoirs of primordial material (Fig. 7i). A large Clapeyron slope can thus prevent pPv from fully covering the CMB region. It is also interesting to note that for large values of Γ_{pPv}, plumes are generated outside reservoirs of primitive material, even for low CMB temperatures (3350 K).

4. Implications for the lower mantle

Several interesting conclusions may be drawn from the numerical experiments discussed in Section 3.

First, increasing the CMB temperature favours large scale reservoirs of dense primordial material. Larger CMB temperature also reduces the stability field of pPv, which becomes thinner and more discontinuous as the CMB temperature increases. On the other hand, increasing CMB temperature promotes the growth of instabilities in the bottom TBL, allowing plumes to rise from regions outside the reservoirs of dense material. Since the low CMB temperature can maintain thin layers of pPv within the hot piles, it should be possible that small lenses of pPv exist at the bottom of large reservoirs (e.g., Lay and Garnero, 2007; Tackley, 2012).

Second, the viscosity of pPv has a strong influence when other parameters (the CMB temperature and Clapeyron slope) allow a substantial amount of pPv to be present above the CMB. In these cases, the stability of the dense reservoirs is strongly affected. For instance, weak pPv, combined with low values of the Clapeyron slope, does not allow large reservoirs of dense material to be maintained, if the CMB temperature is too low. Instead it promotes efficient mixing between dense and regular material, and the presence of a continuous pPv layer around the CMB. We also find that the weak pPv destabilises the margins of the primordial reservoirs, favouring plume generation at their edges. Interestingly, preferential location of plumes at reservoirs edges is in agreement with Paleomagnetic reconstructions of the locations of large igneous provinces (e.g., Burke et al., 2008).

Finally, the Clapeyron slope is a key parameter of the pPv phase change. Increasing its value limits the stability field of pPv, which exists in disconnected patches. It further facilitates the presence of double crossings. In contrast, a low value of the Clapeyron slope allows pPv to spread all over the CMB and if, as mentioned above, the pPv viscosity is very low compared to that of perovskite, reservoirs of dense material are not stable. Fig. 8 shows that a full layer of pPv covering the CMB is determined by two main parameters: the CMB temperature and the Clapeyron slope of the phase change from pv to pPv. Note that although the viscosity contrast between pv and pPv affects the stability of the primordial reservoirs, it has no significant influence on the presence of pPv.

Other model parameters have a strong influence on the stability and shape of primordial dense reservoirs. Here, we choose these parameters according to the results of our previous calculations (Y. Li et al., 2014b), which identified values leading to stable reservoirs. The most important controlling parameter is certainly the buoyancy ratio (measuring the density contrast between dense and

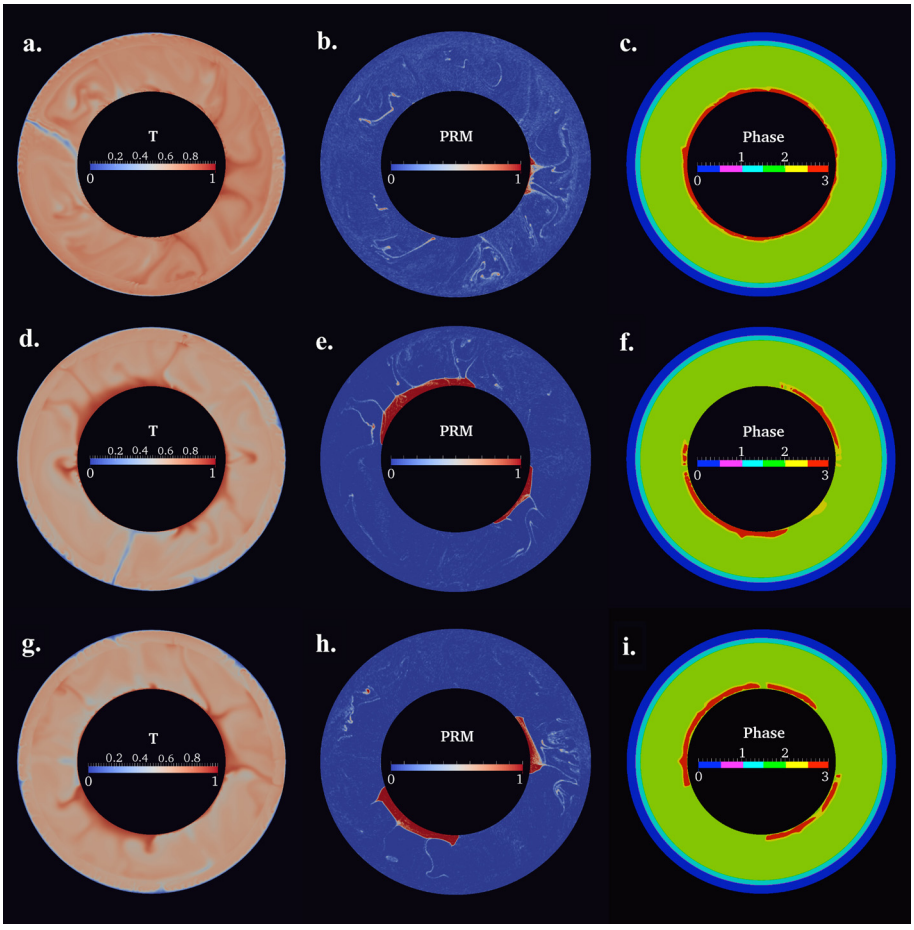

Fig. 6. Snapshots taken at $t = 4.5$ Gyr from cases with weak post-perovskite and $T_{CMB} = 3750$ K. From top to bottom: $\Gamma_{pPv} = 8, 13, 16$ MPa/K, from left to right: superadiabatic temperature, composition, and phase fields. Colour scales are similar to those in Fig. 1. (For interpretation of the references to colour in this figure legend, the reader is referred to the web version of this article.)

regular materials). Previous studies (e.g., McNamara and Zhong, 2005; Deschamps and Tackley, 2009; Y. Li et al., 2014b) suggested that increasing the buoyancy ratio help maintaining primordial reservoirs in the lower mantle. However, it is important to note that the buoyancy ratio should not be chosen too high to avoid full stratification, and to be consistent with density contrast estimates (Trampert et al., 2004; Mosca et al., 2012), around 2% compared to PREM, leading to the buoyancy ratio in the range 0.2–0.4 in our cases. The volume fraction of dense material is less sensitive, and has a limited influence on the stability of reservoirs of dense material (Y. Li et al., 2014b). Large values (10% or more) of this parameter are however not likely because they wouldn't match estimates of LLSVPs' volume, around 4% (Hernlund and Houser, 2008), and because they would lead to a plume distribution (Y. Li et al., 2014b) that does not match paleomagnetic reconstruction of LIPs' locations (Burke et al., 2008). Numerically, the resolution of the grid might also alter the stability of dense reservoir. The resolution we used here (768 lateral nodes and 96 vertical nodes), combined with grid refinement, is enough to avoid this problem.

These findings have interesting implications for the Earth's mantle. First, assuming that the D'' discontinuity is a signature of the pPv phase transition, and noting that this discontinuity is not observed everywhere, pPv is unlikely to be forming a thick continuous layer around the CMB. In our models, such a pPv layer appears for a low value (3350 K) of the CMB temperature and/or a small (8 MPa/K) Clapeyron slope of the pPv phase transition. For the Earth's mantle, larger values of these parameters may thus be preferred. Second, a successful model of mantle convection should explain the presence of LLSVPs by maintaining large scale reservoirs of chemically differentiated material. Models combining weak pPv and low pPv Clapeyron slope are unable to maintain large scale thermo-chemical reservoirs, and instead result in a chemically homogeneous lower mantle that cannot explain structures such as the LLSVPs observed by tomographic models. Therefore, these models appear less likely. Similarly, a low CMB temperature, as suggested by a recent experiment on the solidus of pyrolite (Nomura et al., 2014), should be taken with caution. Results from our models indicate that in order to maintain large primordial reservoirs with such a low CMB temperature, a very large Clapeyron slope is required to avoid a full layer of pPv covering the CMB.

Another important observational constraint is the distribution of plumes. The location of hotspots and paleomagnetic reconstructions of Large Igneous Provinces suggest that plumes are preferentially (but not only) generated on the edges of LLSVPs (e.g., Burke et al., 2008), while a few plumes are originating from regions outside LLSVPs. Our experiments indicate that the development of plumes outside dense reservoirs is mostly controlled by the viscosity contrast between pv and pPv (Section 3.3; Figs. 1 and 3), with weak pPv preventing the generation of such plumes as it favours the spreading of cold downwellings along CMB. In this case, plumes may however be generated outside the dense reservoirs only if the CMB temperature is large. Our experiments further show that high CMB temperature combined with a large Clapeyron slope of the pPv phase transition promote the growth of plumes outside the primordial reservoirs. In contrast, in models with an intermediate CMB temperature (around 3750 K) most

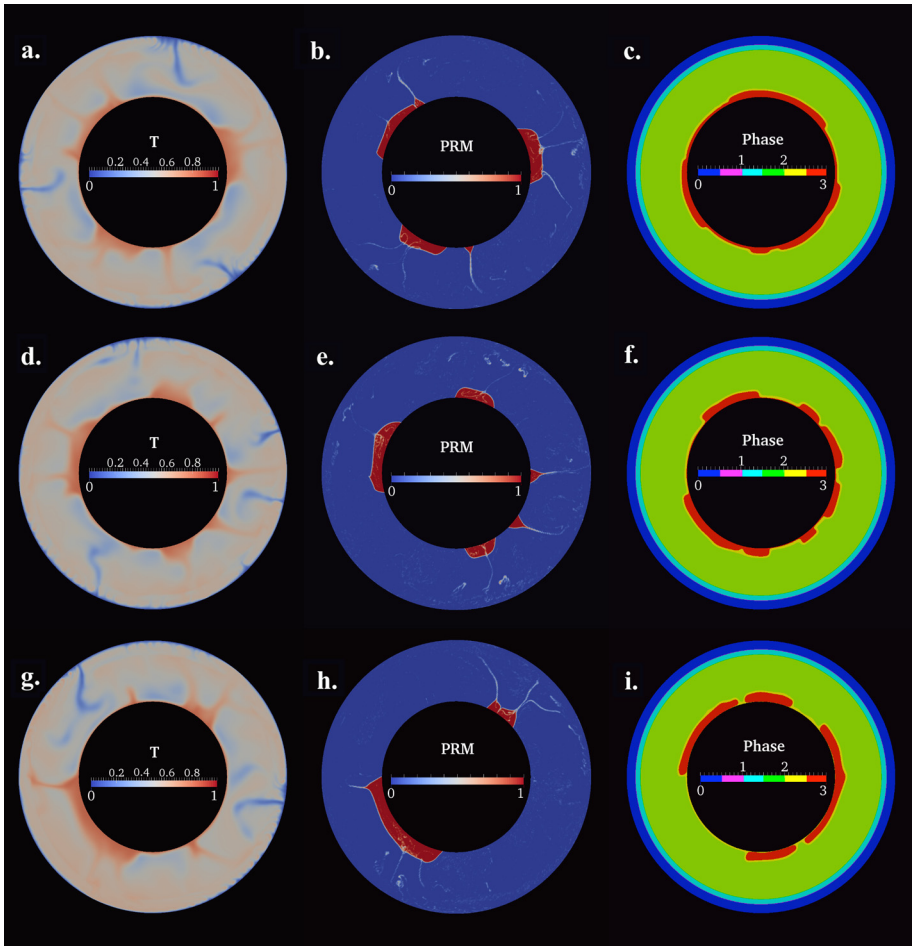

Fig. 7. Snapshots taken at $t = 4.5$ Gyr from cases with regular post-perovskite and $T_{CMB} = 3350$ K. From top to bottom: $\Gamma_{pPv} = 8, 13, 16$ MPa/K, from left to right: superadiabatic temperature, composition, and phase fields. Colour scales are similar to those in Fig. 1. (For interpretation of the references to colour in this figure legend, the reader is referred to the web version of this article.)

plumes originate from the reservoirs of primordial material, and only a few plumes are generated outside these reservoirs, in agreement with observations. One may point out that such instabilities may disappear in experiments with lower Rayleigh numbers than that used in our experiments, and those cases with high CMB temperature may not be totally ruled out. Similarly, increasing the Rayleigh number in models with low or moderate T_{CMB} may lead to the formation of thermal instabilities outside the reservoirs. It should be noted that this would imply substantial modification of the Rayleigh number, whereas in our experiments the reference Rayleigh number was fixed to make the effective Rayleigh number match expected value for the Earth's mantle (typically, in the range 10^6–10^7).

Overall, our experiments indicate that a combination of very low CMB temperature and very small Clapeyron slope is the most unlikely case for the Earth. The CMB temperature shouldn't be too high, as the upper limit for the CMB temperature is the melting temperature of deep mantle material and very high CMB temperature (i.e., 4200 K in this study) leads to long wavelength thermochemical structures in degree-one rather than in degree-two. Furthermore, a high CMB temperature promotes the generation of many plumes outside primordial reservoirs, which contradicts observations. Thus, models of mantle convection that appear to be most likely include a high pPv Clapeyron slope (typically, in the range 13–16 MPa/K), and a moderate CMB temperature (around 3750 K). Additional constrains are required to determine the viscosity contrast between pv and pPv in the range we explored (10^{-3}–1), the viscosity contrast between pv and pPv does not show significant differences on the stability and structure of large primordial reservoirs, but more plumes are being generated outside the large primordial reservoirs in the cases with regular pPv than those with weak pPv.

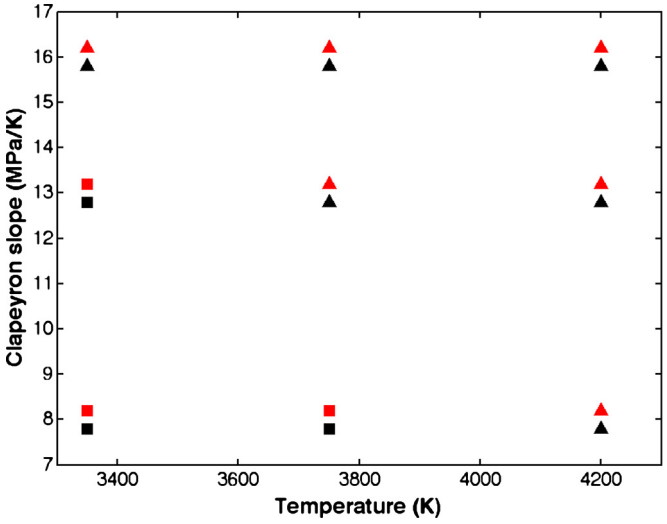

Fig. 8. Observations of whether or not pPv forms a full layer above the CMB. Colour red for regular pPv cases, colour black for weak pPv cases; marker square for pPv observed fully layering above the CMB; marker triangle for not fully layering above the CMB. (For interpretation of the references to colour in this figure legend, the reader is referred to the web version of this article.)

5. Conclusions and perspectives

In this study, we have investigated the effects of the CMB temperature, viscosity contrast between pv and pPv, and Clapeyron slope of the pPv phase change on the distribution and size of the pPv stability field, and on the structure and stability of primordial reservoirs in the lower mantle. The numerical experiments we performed showed that:

1. The CMB temperature has a strong influence on the number and size of reservoirs of primordial material because it controls the mantle temperature, which in turn controls the generation of downwellings below the surface. Lower end temperatures (around 3350 K) favour small size reservoirs, while large scale (degree two) reservoirs appear for higher CMB temperature of around 3750 K and more.

2. In cases with regular pPv, high CMB temperatures (around 4200 K) promote the development of thermal instabilities, and therefore the generation of plumes, outside the reservoirs of primordial materials. On the other hand, weak pPv prevents the formation of such plumes whatever the CMB temperature we tested.

3. Weak (i.e., low viscosity) pPv modifies the stability of the reservoirs of primordial material. This effect is important at small CMB temperature, but remains moderate for intermediate and high temperature (3750 K and higher). Meanwhile, weak pPv strongly prevents the generation of plumes outside large primordial reservoirs.

4. Large values of the Clapeyron slope prevent the formation of a continuous layer of pPv above the CMB. These findings suggest that to explain available geophysical observation, including constraints on the D'' layer, tomographic models, and plume distribution reconstructed from paleomagnetic data, models of mantle dynamics should include a moderate CMB temperature (around 3750 K), and a large Clapeyron slope (13–16 MPa/K) of the pPv phase transition. Our models, on the other hand, do not allow constraining the viscosity of pPv.

Future directions may focus on several aspects. First, it is important to check whether our results, in particular the generation of plumes outside the reservoirs of dense material, are also valid in 3-D spherical geometry, and to compare to observations to find the best fit model. Second, our experiments model subducted slabs in a very simple way that does not take into account the chemistry of slabs. In reality, slabs bring recycled oceanic crust to the bottom of the mantle, which may interact with the reservoirs of primitive material and influence the dynamics of these reservoirs (M. Li et al., 2014; Nakagawa and Tackley, 2014). Third, the phase parameters of the pPv phase change also depend on the composition (e.g., Hirose et al., 2008; Andrault et al., 2010), and more accurate models should take the compositional-dependent phase change into account. Last, with weak pPv, the CMB conductive heat flow is larger than the that with regular pPv, i.e., a mantle with weak pPv might cool down faster than the mantle with regular pPv. Therefore, it will be interesting to include core cooling in future models.

Acknowledgements

We are grateful to the Editor, Bruce Buffet, and the reviewer, Mingming Li, for the constructive review. This work was supported by Swiss National Science Foundation Grants SNF 200021-129510, 200020-149625, Academia Sinica (Taipei, Taiwan) Grant AS-102-CDA-M02, and National Science Council of Taiwan (NSC) Grant 101-2116-M-001-001-MY3. Calculations were run on ETH's brutus cluster. All the data for this study are available upon request to the corresponding author.

Appendix A. Supplementary material

Supplementary material related to this article can be found online at http://dx.doi.org/10.1016/j.epsl.2015.09.040.

References

Ammann, M., Brodholt, J., Wookey, J., Dobson, D., 2010. First-principles constraints on diffusion in lower-mantle minerals and a weak D'' layer. Nature 465, 462–465. http://dx.doi.org/10.1038/nature09052.

Andrault, D., Bolfan-Casanova, N., Nigro, G.L., Bouhifd, M.A., Garbarino, G., Mezouar, M., 2011. Solidus and liquidus profiles of chondritic mantle: implication for melting of the earth across its history. Earth Planet. Sci. Lett. 304, 251–259.

Andrault, D., Muñoz, M., Bolfan-Casanova, N., Guignot, N., Perrillat, J.P., Aquilanti, G., Pascarelli, S., 2010. Experimental evidence for perovskite and post-perovskite coexistence throughout the whole D'' region. Earth Planet. Sci. Lett. 293, 90–96.

Burke, K., Steinberger, B., Torsvik, T.H., Smethurst, M.A., 2008. Plume generation zones at the margins of large low shear velocity provinces on the core–mantle boundary. Earth Planet. Sci. Lett. 265, 49–60. http://dx.doi.org/10.1016/j.epsl.2007.09.042.

Cadek, O., Fleitout, L., 2006. Effect of lateral viscosity variations in the core–mantle boundary region on predictions of the long-wavelength geoid. Stud. Geophys. Geod. 50, 217–232. http://dx.doi.org/10.1007/s11200-006-0013-0.

Caracas, R., Cohen, R.E., 2005. Effect of chemistry on the stability and elasticity of the perovskite and post-perovskite phases in the $MgSiO_3$–$FeSiO_3$–Al_2O_3 system and implications for the lowermost mantle. Geophys. Res. Lett. 32. http://dx.doi.org/10.1029/2005GL023164.

Christensen, U.R., Yuen, D.A., 1985. Layered convection induced by phase transitions. J. Geophys. Res., Solid Earth 90, 10291–10300. http://dx.doi.org/10.1029/JB090iB12p10291.

Cobden, L., Thomas, C., 2013. The origin of D'' reflections: a systematic study of seismic array data sets. Geophys. J. Int. 194, 1091–1118. http://dx.doi.org/10.1093/gji/ggt152.

Davies, D.R., Goes, S., Davies, J., Schuberth, B., Bunge, H.P., Ritsema, J., 2012. Reconciling dynamic and seismic models of Earth's lower mantle: the dominant role of thermal heterogeneity. Earth Planet. Sci. Lett. 353–354, 253–269. http://dx.doi.org/10.1016/j.epsl.2012.08.016.

Deschamps, F., Tackley, P.J., 2008. Searching for models of thermo-chemical convection that explain probabilistic tomography: I. Principles and influence of rheological parameters. Phys. Earth Planet. Inter. 171, 357–373. http://dx.doi.org/10.1016/j.pepi.2008.04.016.

Deschamps, F., Tackley, P.J., 2009. Searching for models of thermo-chemical convection that explain probabilistic tomography. II: influence of physical and compositional parameters. Phys. Earth Planet. Inter. 176, 1–18. http://dx.doi.org/10.1016/j.pepi.2009.03.012.

Fiquet, G., Auzende, A.L., Siebert, J., Corgne, A., Bureau, H., Ozawa, H., Garbarino, G., 2010. Melting of peridotite to 140 Gigapascals. Science 329, 1516–1518. http://dx.doi.org/10.1126/science.1192448.

He, Y., Wen, L., 2012. Geographic boundary of the pacific anomaly and its geometry and transitional structure in the north. J. Geophys. Res., Solid Earth 117. http://dx.doi.org/10.1029/2012JB009436.

Hernlund, J.W., 2010. On the interaction of the geotherm with a post-perovskite phase transition in the deep mantle. Phys. Earth Planet. Inter. 180, 222–234. http://dx.doi.org/10.1016/j.pepi.2010.02.001.

Hernlund, J.W., Houser, C., 2008. On the statistical distribution of seismic velocities in Earth's deep mantle. Earth Planet. Sci. Lett. 265, 423–437. http://dx.doi.org/10.1016/j.epsl.2007.10.042.

Hernlund, J.W., Tackley, P.J., 2008. Modeling mantle convection in the spherical annulus. Phys. Earth Planet. Inter. 171, 48–54. http://dx.doi.org/10.1016/j.pepi.2008.07.037.

Hernlund, J.W., Thomas, C., Tackley, P.J., 2005. A doubling of the post-perovskite phase boundary and structure of the Earth's lowermost mantle. Nature 434, 882–886.

Hirose, K., Takafuji, N., Fujino, K., Shieh, S.R., Duffy, T.S., 2008. Iron partitioning between perovskite and post-perovskite: a transmission electron microscope study. Am. Mineral. 93, 1678–1681.

Hunt, S.A., Weidner, D.J., Li, L., Wang, L., Walte, N.P., Brodholt, J.P., Dobson, D.P., 2009. Weakening of Calcium iridate during its transformation from perovskite to post-perovskite. Nat. Geosci. 2, 794–797.

Hutko, A.R., Lay, T., Revenaugh, J., Garnero, E.J., 2008. Anticorrelated seismic velocity anomalies from post-perovskite in the lowermost mantle. Science 320, 1070–1074. http://dx.doi.org/10.1126/science.1155822.

Ishii, M., Tromp, J., 1999. Normal-mode and free-air gravity constraints on lateral variations in velocity and density of Earth's mantle. Science 285, 1231–1236. http://dx.doi.org/10.1126/science.285.5431.1231.

Karato, S.i., 2011. Rheological structure of the mantle of a super-earth: some insights from mineral physics. Icarus 212, 14–23.

Lay, T., Garnero, E.J., 2007. Reconciling the post-perovskite phase with seismological observations of lowermost mantle structure. In: Post-Perovskite: The Last Mantle Phase Transition, pp. 129–153.

Lekic, V., Cottaar, S., Dziewonski, A., Romanowicz, B., 2012. Cluster analysis of global lower mantle tomography: a new class of structure and implications for chemical heterogeneity. Earth Planet. Sci. Lett. 357–358, 68–77. http://dx.doi.org/10.1016/j.epsl.2012.09.014.

Li, M., McNamara, A.K., Garnero, E.J., 2014. Chemical complexity of hotspots caused by cycling oceanic crust through mantle reservoirs. Nat. Geosci. 7, 366–370.

Li, Y., Deschamps, F., Tackley, P.J., 2014a. Effects of low-viscosity post-perovskite on the stability and structure of primordial reservoirs in the lower mantle. Geophys. Res. Lett. 41, 7089–7097. http://dx.doi.org/10.1002/2014GL061362.

Li, Y., Deschamps, F., Tackley, P.J., 2014b. The stability and structure of primordial reservoirs in the lower mantle: insights from models of thermochemical convection in three-dimensional spherical geometry. Geophys. J. Int. 199, 914–930. http://dx.doi.org/10.1093/gji/ggu295.

Mao, W.L., Campbell, A.J., Prakapenka, V.B., Hemley, R.J., Mao, H.K., 2007. Effect of iron on the properties of post-perovskite silicate. In: Post-Perovskite: The Last Mantle Phase Transition, pp. 37–46.

Masters, G., Laske, G., Bolton, H., Dziewonski, A., 2000. The relative behavior of shear velocity, bulk sound speed, and compressional velocity in the mantle: Implications for chemical and thermal structure. In: Earth's Deep Interior: Mineral Physics and Tomography from the Atomic to the Global Scale, pp. 63–87.

McNamara, A.K., Zhong, S., 2005. Thermochemical structures beneath Africa and the Pacific ocean. Nature 437, 1136–1139.

Mosca, I., Cobden, L., Deuss, A., Ritsema, J., Trampert, J., 2012. Seismic and mineralogical structures of the lower mantle from probabilistic tomography. J. Geophys. Res., Solid Earth 117. http://dx.doi.org/10.1029/2011JB008851.

Murakami, M., Hirose, K., Kawamura, K., Sata, N., Ohishi, Y., 2004. Post-perovskite phase transition in $MgSiO_3$. Science 304, 855–858. http://dx.doi.org/10.1126/science.1095932.

Nakagawa, T., Tackley, P.J., 2005. The interaction between the post-perovskite phase change and a thermo-chemical boundary layer near the core–mantle boundary. Earth Planet. Sci. Lett. 238, 204–216.

Nakagawa, T., Tackley, P.J., 2006. Three-dimensional structures and dynamics in the deep mantle: effects of post-perovskite phase change and deep mantle layering. Geophys. Res. Lett. 33.

Nakagawa, T., Tackley, P.J., 2014. Influence of combined primordial layering and recycled MORB on the coupled thermal evolution of Earth's mantle and core. Geochem. Geophys. Geosyst. 15, 619–633. http://dx.doi.org/10.1002/2013GC005128.

Ni, S., Tan, E., Gurnis, M., Helmberger, D., 2002. Sharp sides to the African superplume. Science 296, 1850–1852. http://dx.doi.org/10.1126/science.1070698.

Nomura, R., Hirose, K., Uesugi, K., Ohishi, Y., Tsuchiyama, A., Miyake, A., Ueno, Y., 2014. Low core–mantle boundary temperature inferred from the solidus of pyrolite. Science 343, 522–525. http://dx.doi.org/10.1126/science.1248186.

Oganov, A.R., Ono, S., 2004. Theoretical and experimental evidence for a post-perovskite phase of $MgSiO_3$ in Earth's D'' layer. Nature 430, 445–448.

Sidorin, I., Gurnis, M., Helmberger, D.V., 1999. Dynamics of a phase change at the base of the mantle consistent with seismological observations. J. Geophys. Res., Solid Earth 104, 15005–15023.

Stackhouse, S., Brodholt, J.P., 2007. The high-temperature elasticity of $MgSiO_3$ post-perovskite. In: Post-Perovskite: the Last Mantle Phase Transition, pp. 99–113.

Tackley, P.J., 2008. Modelling compressible mantle convection with large viscosity contrasts in a three-dimensional spherical shell using the Yin-Yang grid. Phys. Earth Planet. Inter. 171, 7–18. http://dx.doi.org/10.1016/j.pepi.2008.08.005.

Tackley, P.J., 2012. Dynamics and evolution of the deep mantle resulting from thermal, chemical, phase and melting effects. Earth-Sci. Rev. 110, 1–25. http://dx.doi.org/10.1016/j.earscirev.2011.10.001.

Tateno, S., Hirose, K., Sata, N., Ohishi, Y., 2009. Determination of post-perovskite phase transition boundary up to 4400 K and implications for thermal structure in D'' layer. Earth Planet. Sci. Lett. 277, 130–136. http://dx.doi.org/10.1016/j.epsl.2008.10.004.

Trampert, J., Deschamps, F., Resovsky, J., Yuen, D., 2004. Probabilistic tomography maps chemical heterogeneities throughout the lower mantle. Science 306, 853–856. http://dx.doi.org/10.1126/science.1101996.

Tsuchiya, T., Tsuchiya, J., Umemoto, K., Wentzcovitch, R.M., 2004. Phase transition in $MgSiO_3$ perovskite in the Earth's lower mantle. Earth Planet. Sci. Lett. 224, 241–248. http://dx.doi.org/10.1016/j.epsl.2004.05.017.

Wookey, J., Kendall, J.M., Rümpker, G., 2005. Lowermost mantle anisotropy beneath the north Pacific from differential S–ScS splitting. Geophys. J. Int. 161, 829–838.

Yoshino, T., Yamazaki, D., 2007. Grain growth kinetics of $CaIrO_3$ perovskite and post-perovskite, with implications for rheology of D'' layer. Earth Planet. Sci. Lett. 255, 485–493.

Zerr, A., Diegeler, A., Boehler, R., 1998. Solidus of Earth's deep mantle. Science 281, 243–246. http://dx.doi.org/10.1126/science.281.5374.243.